Journal of Power Sources 195 (2010) 8244–8250

Contents lists available at ScienceDirect

Journal of Power Sources

journal homepage: www.elsevier.com/locate/jpowsour

$Li_4Ti_5O_{12}$/Sn composite anodes for lithium-ion batteries: Synthesis and electrochemical performance

Rui Cai, Xing Yu, Xiaoqin Liu, Zongping Shao*

State Key Laboratory of Materials-Oriented Chemical Engineering, College of Chemistry & Chemical Engineering, Nanjing University of Technology, No. 5 Xin Mofan Road, Nanjing 210009, PR China

ARTICLE INFO

Article history:
Received 16 March 2010
Received in revised form 25 July 2010
Accepted 26 July 2010
Available online 3 August 2010

Keywords:
Lithium titanate
Tin oxide
Lithium-ion battery
Anode

ABSTRACT

$Li_4Ti_5O_{12}$/tin phase composites are successfully prepared by cellulose-assisted combustion synthesis of $Li_4Ti_5O_{12}$ matrix and precipitation of the tin phase. The effect of firing temperature on the particulate morphologies, particle size, specific surface area and electrochemical performance of $Li_4Ti_5O_{12}$/tin oxide composites is systematically investigated by SEM, XRD, TG, BET and charge–discharge characterizations. The grain growth of tin phase is suppressed by forming composite with $Li_4Ti_5O_{12}$ at a calcination of 500 °C, due to the steric effect of $Li_4Ti_5O_{12}$ and chemical interaction between $Li_4Ti_5O_{12}$ and tin oxide. The experimental results indicate that $Li_4Ti_5O_{12}$/tin phase composite fired at 500 °C has the best electrochemical performance. A capacity of 224 mAh g^{-1} is maintained after 50 cycles at 100 mA g^{-1} current density, which is still higher than 195 mAh g^{-1} for the pure $Li_4Ti_5O_{12}$ after the same charge/discharge cycles. It suggests $Li_4Ti_5O_{12}$/tin phase composite may be a potential anode of lithium-ion batteries through optimizing the synthesis process.

1. Introduction

Lithium-ion batteries have been widely applied as power sources of personal electronic devices. To compare with many other electrochemical energy storage devices, they have the advantages of no memory effect, high cell voltage, no toxic materials, and high volumetric and gravimetric energy density [1,2]. With the ever diminishing resources of fossil fuels and increasing environmental pollutant emissions from the combustion of fossil fuels, nowadays there are considerable interests from all over the world in electric vehicles and electric-hybrid vehicles with lithium-ion batteries as the potential power sources [3,4].

State-of-the-art lithium-ion batteries are based on carbon or graphite anode, which has a theoretical discharge capacity of 372 mAh g^{-1} and a lithium-insertion potential (or end-of-Li-insertion potential) approaching 0 V (vs. Li/Li^+) [5–7]. Such a low potential ensures a high cell voltage, however, it also introduces safety problem when the cell is over charged. Spinel-type $Li_4Ti_5O_{12}$ oxide has been considered as a promising alternative material to current carbon/graphite anode [8–15]. It follows a two-phase mechanism for the lithium-ion insertion and extraction electrochemical reactions as follows [16]:

$$(\text{Discharge})Li_4Ti_5O_{12} + 3Li^+ + 3e^- \leftrightarrow Li_7Ti_5O_{12}(\text{charge}) \quad (1)$$

The Li-insertion (discharge) process happens at ~1.5 V vs. Li^+/Li that has much better safety characteristics. Furthermore, during the lithium intercalation and de-intercalation processes there is almost no change in cell volume [17], this is beneficial for a long cycling lifetime. However $Li_4Ti_5O_{12}$ has a relatively low theoretical capacity of 175 mAh g^{-1}. It also has low electronic conductivity, as a result, poor rate performance was often observed for coarse $Li_4Ti_5O_{12}$ anode [18]. Decreasing the particle size or surface coating with a more conductive material such as carbon and silver are the general ways to improve the rate performance of $Li_4Ti_5O_{12}$ anode [19–21].

On the other hand, tin oxides (SnO and SnO_2) have received considerable attentions as anode materials of Li-ion batteries recently [22–25]. The reaction mechanism during the charge and discharge processes in the case of SnO_2 anode can be expressed as:

$$4Li^+ + 4e^- + SnO_2 \rightarrow 2Li_2O + Sn \quad (\text{irreversible}) \quad (2)$$

$$xLi^+ + xe^- + Sn \rightarrow Li_xSn (0 \le x \le 4.4) \quad (\text{reversible}) \quad (3)$$

Based on above reaction mechanism, theoretically the first discharge capacity of SnO_2 reaches as high as 1491 mAh g^{-1}. Since only the second reaction is reversible, the reversible discharge capacity of SnO_2 is 781 mAh g^{-1} based on the mass of SnO_2, which is still more than two times that of graphite and several times that of $Li_4Ti_5O_{12}$. However, a large volume variation is experienced for metallic tin during the alloying and de-alloying processes. The volume expansion can reach as large as 300% when tin alloys with lithium with the formation of $Li_{4.4}Sn$ [26]. Such a large volume

* Corresponding author. Tel.: +86 25 83172256; fax: +86 25 83172256.
E-mail address: shaozp@njut.edu.cn (Z. Shao).

0378-7753/$ – see front matter © 2010 Elsevier B.V. All rights reserved.
doi:10.1016/j.jpowsour.2010.07.059

change could cause the detachment of electrode from current collector or the pulverization of electrode materials, as a result, a fast decay in capacity with cycling times for the tin oxide anodes is frequently observed [27–29]. Decreasing particle size of tin oxides to the nanometer level can obviously increase the cycling stability. However, the electric wiring of nano-particles becomes a big challenge [30].

A matrix is proposed for the nano-tin particles, which could not only increase the current collecting efficiency of the electrode, but also act as a buffer to accommodate the volume expansion of Sn during the charge/discharge processes, and consequently, an obvious improvement in the cycling performance is expected [31–34]. An innovative ideal is to apply $Li_4Ti_5O_{12}$ as such a matrix for Sn particles. On the other hand, the metallic Sn may in turn modify the properties of $Li_4Ti_5O_{12}$ because of its high electrical conductivity. Thereby, a synergistic effect between $Li_4Ti_5O_{12}$ and Sn may be created. However, up to now only one related work was available in the literature. Hao et al. conducted the primary investigation of $Li_4Ti_5O_{12}/SnO_2$ composite materials for anodes of lithium-ion batteries [35]. Their electrochemical results indicated that the formation of $Li_4Ti_5O_{12}/SnO_2$ composites increased the reversible capacity of $Li_4Ti_5O_{12}$ and cycling reliability of the SnO_2 anode material.

In this paper, we reported the advanced synthesis and systematic investigation of $Li_4Ti_5O_{12}$/tin oxide composites as potential anodes of lithium-ion batteries. Importance was paid to the effect of firing temperature on the phase formation, particle size and electrochemical performance of the resulted composite anodes, the synergistic effect between $Li_4Ti_5O_{12}$ and Sn was discussed.

2. Experimental

$Li_4Ti_5O_{12}$ was synthesized by a cellulose-assisted combustion technique with $LiNO_3$ and tetra butyl titanate [$Ti(C_4H_9O)_4$] as Li and Ti cation sources, respectively. De-waxed cotton fiber, pre-treated by 67 wt.% concentrated nitric acid for 1 h, was applied as the cellulose raw material. The detailed preparation procedure can refer to our previous publication [36]. $Li_4Ti_5O_{12}$/tin oxide composites were synthesized by first precipitating $SnO{\cdot}xH_2O$ into the matrix of $Li_4Ti_5O_{12}$ and then firing at elevated temperature. Tin(II) chloride was first dissolved in 40 mL absolute ethanol at room temperature, and then $Li_4Ti_5O_{12}$ powder, at the weight ratio of $Li_4Ti_5O_{12}$ to metallic Sn of 9:1, was added into the $SnCl_2$ solution, after the agitation for 20 min, NH_4OH was slowly dropped into the suspension under stirring until pH reached 10 to induce the precipitation, the as-obtained slurry was washed by deionized water, and then dried at 80 °C for 4 h, the solid precursor was transferred into an alumina crucible and calcined at different temperatures for 3 h.

Electrode paste, made of 85 wt.% $Li_4Ti_5O_{12}$/tin oxide composite, 9 wt.% conductive Super P (NCM HERSBIT Chemical Co. Ltd., China) and 8 wt.% PVDF (polyvinylidenedifluoride; Aldrich), was painted on a Cu foil, which acts as the current collector. The electrode was then punched into disks with a diameter of 10 mm and then dried at 100 °C for 24 h under vacuum. Half cells were assembled by applying the disk-shape electrode as the anode, a liquid mixture composed of 1 M $LiPF_6$/ethylene carbonate (EC)/propylene carbonate (PC)/diethyl carbonate (DEC) (1:1:1 by volume) as the electrolyte, a microporous polypropylene film (Celgard 2400) as the separator, and lithium foil as the counter electrode. The cell assembly was conducted in a glove box filled with pure argon.

Phase composition of $Li_4Ti_5O_{12}$/tin oxide powders obtained was characterized by X-ray diffraction (XRD, Bruker D8 advance diffractometer with filtered Cu Kα radiation). The morphologies of the samples were observed by scanning electron microscopy (SEM, HITACHI S-4800). The decomposition behavior of precipitated $SnO{\cdot}xH_2O$ was examined by a NETZSCH STA 409PC thermogravimetry in the temperature range of 25–800 °C at a heating rate of 10 °C min^{-1} and under a flowing nitrogen atmosphere. The specific surface area was measured by the BET method at the temperature of liquid nitrogen using a BELSORP II surface analyzer. The charge–discharge characteristics of the cells were recorded over the potential range between 0.5 and 3.0 V using a NEWARE BTS-5V50mA computer-controlled battery test station.

3. Results and discussions

3.1. Synthesis

After the addition of NH_4OH solution into $SnCl_2$–$Li_4Ti_5O_{12}$ suspension, the following precipitation reaction was induced:

$$SnCl_2{\cdot}2H_2O + 2NH_4OH \rightarrow SnO{\cdot}xH_2O\downarrow + (3-x)H_2O + 2NH_4Cl \quad (4)$$

To demonstrate the amount of hydrate water (x) in $SnO{\cdot}xH_2O$ compound and the required temperature for the complete elimination of hydrate water, after filtering and drying, the $Li_4Ti_5O_{12}/SnO_2{\cdot}xH_2O$ composite was conducted thermal gravimetric analysis (TGA) in an inert gas atmosphere, for comparison the TGA profile of $SnO_2{\cdot}xH_2O$ compound prepared from the similar precipitation process was also presented. As shown in Fig. 1, for the pure $SnO_2{\cdot}xH_2O$, the weight loss started at room temperature and finished at ~400 °C with a total weight loss of ~8.7 wt.%, then a very weak weight gain was observed with the further increase of temperature. It suggests that thermal decomposition of pure $SnO{\cdot}xH_2O$ was completed at around 400 °C. Based on the weight loss, the water content x in $SnO{\cdot}xH_2O$ was determined to be around 0.71. The weak weight gain with the further increase of temperature at higher than 400 °C can be explained by the oxidation of tin phase by trace amount of oxygen presented in the inert gas. For the $Li_4Ti_5O_{12}/SnO{\cdot}xH_2O$ precursor, the weight loss was completed at around 320 °C, lower than the decomposition temperature of pure $SnO{\cdot}xH_2O$ phase. It suggests certain type of interaction between $SnO{\cdot}xH_2O$ and $Li_4Ti_5O_{12}$ phases was likely existed in $Li_4Ti_5O_{12}/SnO{\cdot}xH_2O$ composite, which promoted the decomposition of $SnO{\cdot}xH_2O$. Based on the weight loss, the x in $Li_4Ti_5O_{12}/SnO{\cdot}xH_2O$ was found to be around 0.9. Based on Eq. (4) and Fig. 1, the content of $Li_4Ti_5O_{12}$ in $Li_4Ti_5O_{12}/SnO{\cdot}xH_2O$ composite is 87.66, 88.07 and 88.84 wt.% at various temperatures of 40, 200 and 400 °C, respectively.

Fig. 2 shows XRD patterns of the as-synthesized $Li_4Ti_5O_{12}$, $Li_4Ti_5O_{12}/SnO{\cdot}xH_2O$ precursor, and the products from the further

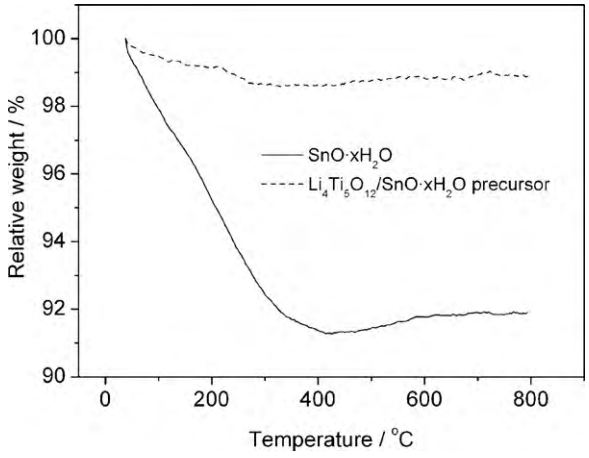

Fig. 1. TG curves of $Li_4Ti_5O_{12}/SnO{\cdot}xH_2O$ and $SnO{\cdot}xH_2O$ solid precursor under a nitrogen atmosphere with a heating rate of 10 °C min^{-1}.

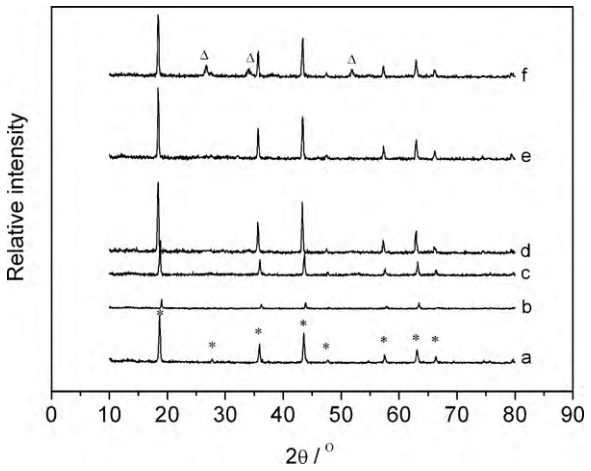

Fig. 2. XRD patterns of as-synthesized $Li_4Ti_5O_{12}$ oxide (700 °C calcined) (a), $Li_4Ti_5O_{12}$/SnO·xH$_2$O precursor (b), and the products (c–f) from further calcination of the $Li_4Ti_5O_{12}$/SnO·xH$_2$O precursor at 400–700 °C in nitrogen (* – $Li_4Ti_5O_{12}$; Δ – rutile SnO_2).

calcination of $Li_4Ti_5O_{12}$/SnO·xH$_2$O precursor in an inert atmosphere at various temperatures for 3 h. All the diffraction peaks of the as-synthesized $Li_4Ti_5O_{12}$ sample, prepared by the cellulose-assisted combustion synthesis with a following calcination step at 700 °C in air for 5 h, can be indexed well based on a spinel-type phase structure, suggesting the successful formation of phase-pure $Li_4Ti_5O_{12}$ oxide. For the $Li_4Ti_5O_{12}$/SnO·xH$_2$O precursor, only the $Li_4Ti_5O_{12}$ phase was detected. It suggests SnO·xH$_2$O in the composite formed from the precipitation process is likely in amorphous structure. When the calcination temperature is between 400 and 600 °C, there was still no crystallized tin oxide phase detectable by XRD. However, with the further increase of firing temperature to 700 °C, besides the main $Li_4Ti_5O_{12}$ spinel phase, some additional diffraction peaks, which can be assigned to the rutile SnO_2 phase, were also observed. SnO is not stable at elevated temperature, it was reported that initial disproportionation occurs to give Sn metal and Sn_3O_4 which further reacts to give SnO_2 and Sn metal when SnO is heated in an inert atmosphere [37].

$$4SnO \rightarrow Sn_3O_4 + Sn \quad (5)$$

$$Sn_3O_4 \rightarrow 2SnO_2 + Sn \quad (6)$$

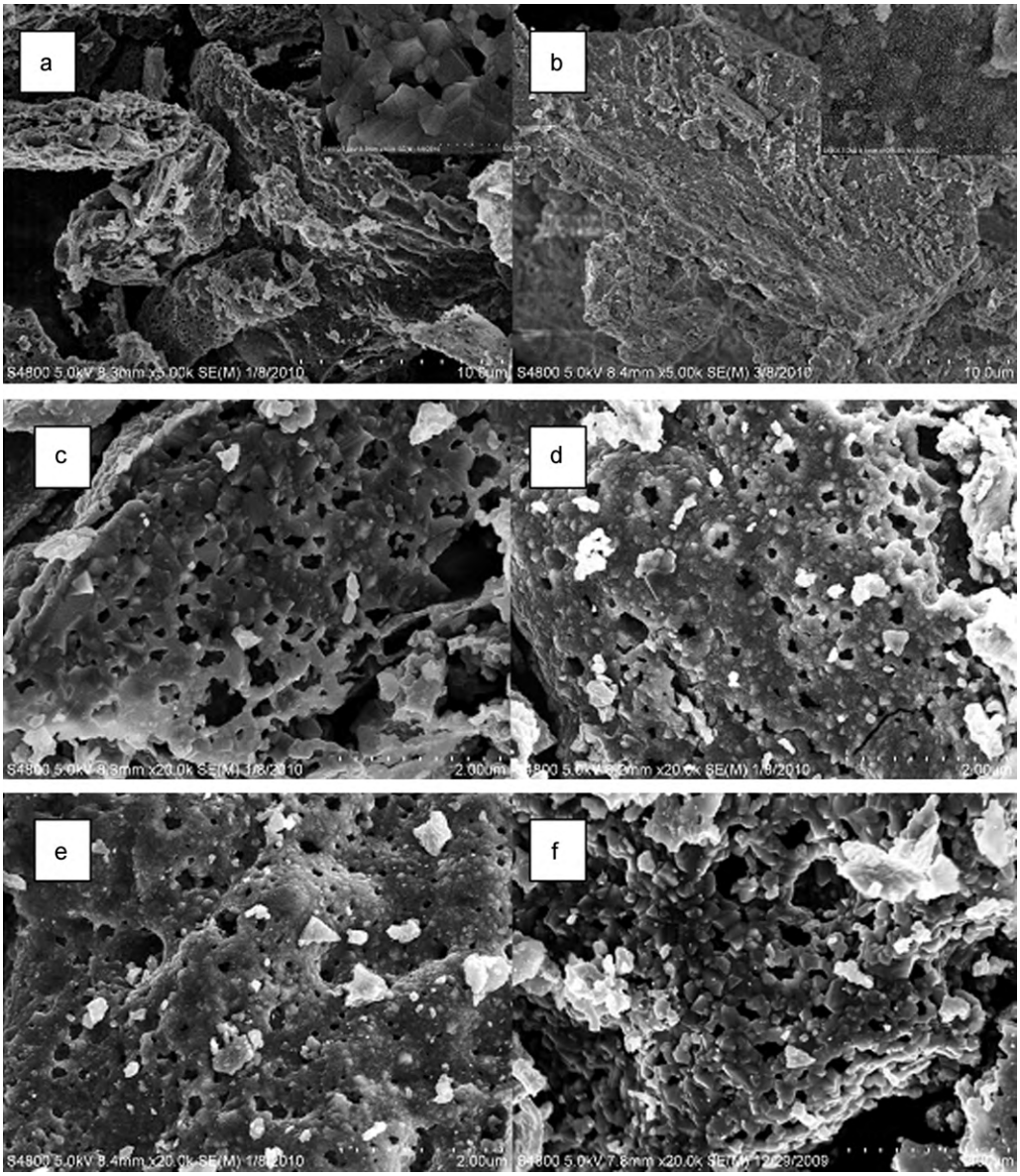

Fig. 3. SEM photos of $Li_4Ti_5O_{12}$ (a), $Li_4Ti_5O_{12}$/tin phase precursor (b) and $Li_4Ti_5O_{12}$/tin phase calcined at various temperatures (c–f): (c) 400 °C, (d) 500 °C, (e) 600 °C and (f) 700 °C.

Table 1
The specific surface area of the $Li_4Ti_5O_{12}$, $Li_4Ti_5O_{12}$/tin phase composite and pure tin phase.

	$Li_4Ti_5O_{12}$	$Li_4Ti_5O_{12}$/tin phase composite			
Temperature (°C)	700	400	500	600	700
Specific surface area ($m^2\,g^{-1}$)	8.4	15.2	13.1	9.8	5.5
Specific surface area ($m^2\,g^{-1}$) (calculated)	–	15.2	10.5	10	9.6
	$Li_4Ti_5O_{12}$*	Pure tin phase (experiment)			
Temperature (°C)	700	400	500	600	700
Specific surface area ($m^2\,g^{-1}$)	7.3	77.5	35.6	31.6	27.9
Grain size (nm)	236	12.1	26.3	29.7	33.6
Coverage	–	43%	20%	17%	10%
	$Li_4Ti_5O_{12}$/tin phase precursor	Tin phase in $Li_4Ti_5O_{12}$/tin phase composite (calculated)			
Temperature (°C)	–	400	500	600	700
Specific surface area ($m^2\,g^{-1}$)	24.3	77.8	59.1	29.6	–
Grain size (nm)	–	12	15.9	31.7	–

* The product from further calcination of the $Li_4Ti_5O_{12}$/$SnO{\cdot}xH_2O$ precursor at 400–700 °C in nitrogen.

It then well explains the appearance of SnO_2 phase instead of SnO in $Li_4Ti_5O_{12}$/tin phase composite after the calcination at 700 °C. In the later discussion, for simplicity, the SnO_2 and Sn mixture in the composite was named as tin phase.

Fig. 3 shows the SEM photos of single-phase $Li_4Ti_5O_{12}$ and $Li_4Ti_5O_{12}$/tin phase composites fired at various temperatures. The $Li_4Ti_5O_{12}$ oxide contained large amount of pores in micrometer level. After the introduction of $SnO{\cdot}xH_2O$ phase, the number of these pores is much reduced. The pores are likely filled with $SnO{\cdot}xH_2O$ after the precipitation. After the firing at 400–700 °C the grain grew, especially the firing at 700 °C.

The BET specific surface areas of single-phase $Li_4Ti_5O_{12}$ (material for the preparation of $Li_4Ti_5O_{12}$/tin phase composite), the $Li_4Ti_5O_{12}$ oxide after the further calcination at 700 °C for 3 h in an inert atmosphere, and the various $Li_4Ti_5O_{12}$/tin phase composites calcined at different temperatures in an inert atmosphere for 3 h were measured (Table 1). For comparison, the specific surface area of pure tin phase prepared from the similar precipitation process was also analyzed. Single-phase $Li_4Ti_5O_{12}$ has a BET specific surface area of ~8.4 $m^2\,g^{-1}$. After the further firing at 700 °C for 3 h in an argon atmosphere, its specific surface area reduced only slightly to ~7.3 $m^2\,g^{-1}$. After the introduction of $SnO{\cdot}xH_2O$ phase, the specific surface area of the $Li_4Ti_5O_{12}$/$SnO{\cdot}xH_2O$ composite reached 24.3 $m^2\,g^{-1}$. Such obvious increment in surface area was clearly contributed from the $SnO{\cdot}xH_2O$ phase. The surface area of $Li_4Ti_5O_{12}$/tin phase composite decreased monotonously with calcination temperature. It is 15.2, 13.1, 9.8 and 5.5 $m^2\,g^{-1}$ after the calcination at 400, 500, 600 and 700 °C for 3 h, respectively. For the pure tin phase, its specific surface area is 77.5, 35.6, 31.6 and 27.9 $m^2\,g^{-1}$ at a calcination temperature of 400, 500, 600 and 700 °C, respectively. Assuming no any interaction between $Li_4Ti_5O_{12}$ and tin phase, the surface area of $Li_4Ti_5O_{12}$/tin phase composite can be calculated based on the respective surface area of the $Li_4Ti_5O_{12}$ and tin oxide phases. For simplicity, the surface area of $Li_4Ti_5O_{12}$ phase is treated as 7.3 $m^2\,g^{-1}$ at all calculations. The calculated surface area of $Li_4Ti_5O_{12}$/tin phase composite is 15.2, 10.5, 10.0 and 9.6 $m^2\,g^{-1}$, respectively, at a calcination temperature of 400, 500 and 600 and 700 °C. At a calcination temperature of 400 °C, the measured surface area of the composite matched pretty well with the calculated value, it implies there was no mutual effect on the particle size between $Li_4Ti_5O_{12}$ and tin phase at 400 °C. However, when the calcination temperature was elevated to 500 or 600 °C, the measured surface area of $Li_4Ti_5O_{12}$/tin phase composite is higher than that calculated. It is likely the grain growth of tin phase was suppressed by forming composite with $Li_4Ti_5O_{12}$. Two mechanisms are possible for such suppressing effect. One is the steric effect created by the porous structure of substrate. Previously we have demonstrated that $Li_4Ti_5O_{12}$ was full of macropores in micrometer level. As shown in Fig. 4 is the isothermal adsorption curve of the as-prepared $Li_4Ti_5O_{12}$. There are almost negligible amount of micropores and mesopores in $Li_4Ti_5O_{12}$. The tin phase was then likely confined in the macropores of $Li_4Ti_5O_{12}$, which effectively reduced the opportunity of the tin phase to aggregate. The other is the chemical interaction between the substrate and the supported material, which can effectively reduce the mobility of the supported material (tin phase in this study). Previously we have demonstrated that certain type of interaction between $Li_4Ti_5O_{12}$ and tin phase likely existed within the $Li_4Ti_5O_{12}$/tin phase composite by the TG analysis.

At a calcination of 700 °C, however, the measured specific surface area of the composite is much lower than that calculated. According to the SEM examination (Fig. 3), the composite fired at 700 °C was much more sintered than those calcined at 400–600 °C. It implies the tin phase facilitated the sintering and the grain growth of the $Li_4Ti_5O_{12}$ main phase. Previously, it was reported that some oxides such as CuO and ZnO can perform as sintering aid of many composite oxides [38–40]. The tin phase likely acted as a sintering aid for $Li_4Ti_5O_{12}$. Such effect was negligible at 400–600 °C, while it was noticeable at 700 °C.

3.2. Electrochemical performance

Fig. 5 shows the first discharge-charge curves of the various $Li_4Ti_5O_{12}$/tin phase composites from the firing at 400–700 °C for 3 h, performed at a constant current density of 100 mA g^{-1} and in the voltage range of 0.5–3.0 V, for comparison, the curves for

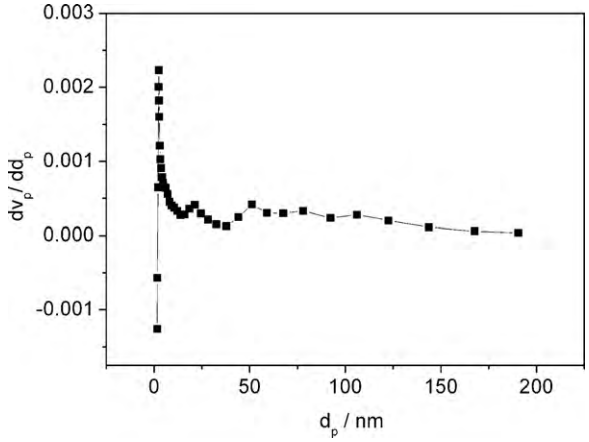

Fig. 4. Isothermal adsorption curves of the as-prepared $Li_4Ti_5O_{12}$ (calcined at 700 °C for 5 h)

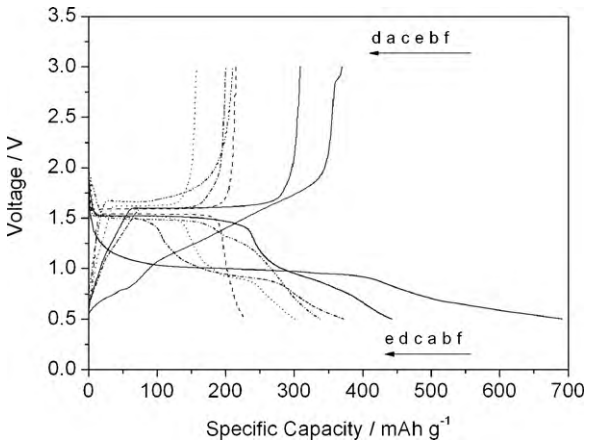

Fig. 5. First charge/discharge curves of the cell with $Li_4Ti_5O_{12}$, SnO_2 and various $Li_4Ti_5O_{12}$/tin phase composites at 100 mA g^{-1} between 0.5 and 3.0 V ((a, b, c and d) $Li_4Ti_5O_{12}$/tin phase composite calcined at 400, 500, 600 and 700 °C, respectively; (e) $Li_4Ti_5O_{12}$ and (f) SnO_2).

the single-phase $Li_4Ti_5O_{12}$ and tin phase prepared from precipitation method after the further calcination at 500 °C for 3 h in an inert atmosphere (tin phase-500) were also presented. For the pure $Li_4Ti_5O_{12}$ oxide, only one discharge plateau (~1.50 V) was observed, a character of the two-phase lithium insertion process. A first discharge capacity and charge capacity of 226 and 214 mAh g^{-1} was obtained for $Li_4Ti_5O_{12}$, with a coulombic efficiency of 95%. The excellent electrochemical reversibility of pure $Li_4Ti_5O_{12}$ is attributed to its near zero volume change during the lithium insertion/extraction processes [41]. For the pure tin phase, a first discharge capacity and charge capacity of 690 and 370 mAh g^{-1}, respectively, was achieved with a coulombic efficiency of only 54%. Such low coulombic efficiency can be attributed to the irreversible lithium insertion into SnO_2 with the formation of Sn and also the large volume change of the lithium insertion into metallic Sn anode. The relatively low discharge capacity of the tin phase in this study as compared to the theoretical value of ~1491 mAh g^{-1} is due to the high ending discharge voltage applied in current investigation (0.5 V). The formation of Li_xSn alloy occurred largely at a voltage lower than 0.5 V based on the literature results [42]. As compared to the single-phase $Li_4Ti_5O_{12}$ anode, the first discharge capacity was all improved for the various composites calcined at different temperatures. Such improvement can be explained by the much higher first discharge capacity of tin phase than $Li_4Ti_5O_{12}$. However, a significant effect of the firing temperature on the first discharge capacity of the composite was observed. The composite from firing at 500 °C had the highest capacity of around 442 mAh g^{-1}, followed by the sample fired at 400 °C with a capacity of around 372 mAh g^{-1}, while the sample fired at 700 °C demonstrated the lowest capacity of ~300 mAh g^{-1}. The effect of firing temperature on particle size and specific surface area is very important. The surface area of the $Li_4Ti_5O_{12}$/tin oxide composite decreased monotonously and the grain size increased monotonously with calcination temperature. Higher surface area and smaller grain size will decrease diffusion length and increase contact area between the active materials and electrolyte which will enhance electrochemical performance of the composites.

For all $Li_4Ti_5O_{12}$/tin oxide composites calcined at different temperatures, two discharge plateaus were observed, one around 1.5 V and the other around 1.0 V. Based on the discharge characteristics of $Li_4Ti_5O_{12}$ and tin oxide, the first one is likely related to lithium insertion into the $Li_4Ti_5O_{12}$ phase with the formation of $Li_7Ti_5O_{12}$, while the second one is associated with the lithium insertion into SnO_2 with the formation of metallic Sn and Li_2O in the composite. According to Fig. 5, the discharge capacity of the plateau at around 1.5 V is 79, 206, 181 and 115 mAh g^{-1} for the composites calcined at 400, 500, 600 and 700 °C, respectively. The discharge capacity at 1.5 V for the sample calcined at 500 °C even exceeded that of pure $Li_4Ti_5O_{12}$ (179 mAh g^{-1}) according to the discharge profiles of pure $Li_4Ti_5O_{12}$ anode in Fig. 5. It suggests a synergistic effect between $Li_4Ti_5O_{12}$ and tin oxide likely happened in this composite. According to Fig. 5, the composites calcined at 600 and 500 °C likely had the strongest interaction between $Li_4Ti_5O_{12}$ and the tin phase. The much less discharge capacity for the composite fired at 700 °C can be explained by the increased grain size of the $Li_4Ti_5O_{12}$, as demonstrated by the BET surface area measurement and SEM characterization.

It is interesting that the sample fired at 400 °C has the smallest first discharge capacity at around 1.5 V, while it has the largest capacity at around 1.0 V among the others. Because the charge/discharge processes involve the electron transfer, the anode particles need to be effectively wired by the conductive additive, the isolated particles will be electrochemically inactive. The $Li_4Ti_5O_{12}$/tin phase composite can be wired either via the $Li_4Ti_5O_{12}$ phase or via the tin phase. Since SnO_2 is a semiconductor and the formation of metallic Sn happens mainly at a voltage of around 0.9–1.0 V, during the first discharge process, the $Li_4Ti_5O_{12}$ in the composite that was wired through SnO_2 phase did not contribute to the capacity during the first discharge process. The smallest first discharge capacity at the voltage platform of ~1.5 V for the composite fired at 400 °C implies it had the least particle wiring through the $Li_4Ti_5O_{12}$ phase among the various $Li_4Ti_5O_{12}$/tin phase composites calcined at different temperatures.

To support above assumption, the coverage of the $Li_4Ti_5O_{12}$ oxide by tin phase was estimated based on the BET surface area. For simplicity, the tin phase is still treated as SnO instead of a mixture of Sn and SnO_2, while the specific surface area of $Li_4Ti_5O_{12}$ in $Li_4Ti_5O_{12}$/tin phase composites was treated as 7.3 m^2 g^{-1} at all calcination temperatures. The specific surface area of the tin phase (SnO) was calculated based on the surface area of the composite. It turns out to be 77.8, 59.1 and 29.6 m^2 g^{-1} at a calcination temperature of 400, 500 and 600 °C, respectively (Table 1). Assuming the sphere shape for the tin phase in $Li_4Ti_5O_{12}$/tin phase composites, the grain size of SnO was calculated to be 12.0, 15.9 and 31.7 nm at a calcination temperature of 400, 500 and 600 °C, respectively. Assuming the compact packing in monolayer of the SnO phase over the $Li_4Ti_5O_{12}$ surface, the surface coverage was calculated to be 43%, 20% and 17%, respectively, at a calcination temperature of 400, 500 and 600 °C. It shows that large part of the $Li_4Ti_5O_{12}$ surface was indeed covered by the tin phase for the composite calcined at 400 °C, however, the coverage quickly reduced to only 20% when the firing temperature was elevated to 500 °C.

After the first discharge process, the composites were conducted the charge process at the same current density of 100 mA g^{-1} between 0.5 and 3.0 V. As to the first charge capacity, the sample fired at 500 °C still showed the highest value among the others. It reached a capacity of around 310 mAh g^{-1} with a coulombic efficiency of 70%. Although a higher first discharge capacity was observed for the composite prepared from the calcination at 400 °C than that calcined at 600 °C, a higher first charge capacity was observed for the 600 °C calcined one instead. As mentioned, the composite fired at 400 °C likely had the largest portion of the particles being wired through the Sn phase. Due to the large volume changes associated with the alloy and de-alloy processes of metallic tin, a large capacity loss was occurred during the charge process. It then explains the smaller charge capacity of the 400 °C calcined composite than the 600 °C calcined one.

Fig. 6 shows the cycling performance of various $Li_4Ti_5O_{12}$/tin phase composites from the calcination at different temperatures. Again, the composite from the calcination at 500 °C showed the best cycling stability, after 50 cycles at a charge–discharge cur-

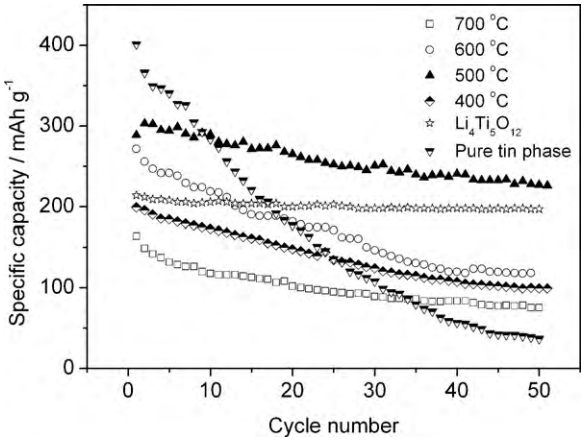

Fig. 6. Cycling performance of $Li_4Ti_5O_{12}$, pure tin phase and various $Li_4Ti_5O_{12}$/tin phase composites at 100 mA g^{-1} between 0.5 and 3.0 V.

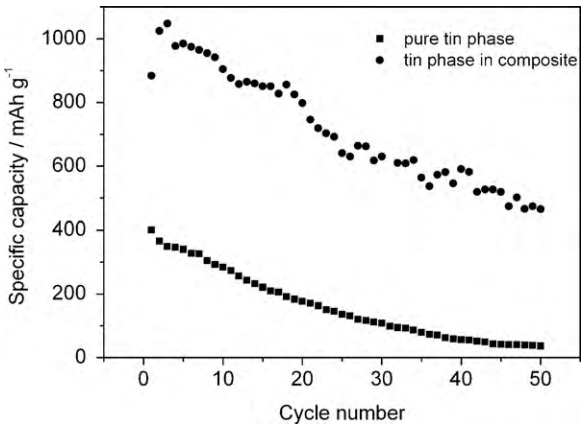

Fig. 7. Cycling characteristics of pure tin phase (500 °C calcined) and the tin phase in $Li_4Ti_5O_{12}$/tin phase composite (500 °C calcined) from 0.5 to 3 V at 100 mA g^{-1} current density.

rent density of 100 mA g^{-1}, a discharge capacity of 224 mAh g^{-1} was maintained, which is still higher than 196 mAh g^{-1} for the pure $Li_4Ti_5O_{12}$ after 50 charge–discharge cycles at the same current density. However, the composites fired at 400, 600 and 700 °C had capacities of only 100, 120 and 76 mAh g^{-1} after 50 cycles, respectively. It further demonstrated the significant effect of the firing temperature on the performance of $Li_4Ti_5O_{12}$/tin oxide composite. As shown in Fig. 6 is cycling time dependence of the discharge capacity of $Li_4Ti_5O_{12}$/tin phase composite, for comparison the data of pure $Li_4Ti_5O_{12}$ anode and tin phase anode were also presented. The cycling stability of the composite is much improved as compared to the pure tin phase, while it is slightly worse than the pure $Li_4Ti_5O_{12}$. This trend is more clearly demonstrated in Table 2. After the cycling at the same current density of 100 mA g^{-1} for 50 cycles, the capacity retention is 92.9%, 74.6% and 12.4% for pure $Li_4Ti_5O_{12}$, $Li_4Ti_5O_{12}$/tin phase composite and tin oxide, respectively.

For the $Li_4Ti_5O_{12}$/tin phase composite anode, the capacity was contributed from both the $Li_4Ti_5O_{12}$ phase and the Sn phase. After the first cycle, the SnO_2 phase in the composite anode was successfully irreversibly reduced to metallic Sn, during the following cycling process, the capacity associated with the plateau at around 1.5 V was mainly contributed from the $Li_4Ti_5O_{12}$ phase. Assuming the ratio of the plateau capacity at around 1.5 V to the total capacity of $Li_4Ti_5O_{12}$ between 0.5 and 3.0 V does not change with the cycling time, the capacity contributed from the $Li_4Ti_5O_{12}$ phase in the composite can be estimated from the plateau capacity, while the capacity contributed from the Sn phase can be obtained by substitution of the capacity of $Li_4Ti_5O_{12}$ from the total capacity of the composite. Fig. 7 gives out of a comparison of cycling performance of pure tin phase and the tin phase in the composite. It clearly shows that the cycling stability of $Li_4Ti_5O_{12}$ phase is slightly reduced while the cycling stability of the tin phase was greatly improved after the formation of composite with $Li_4Ti_5O_{12}$ oxide. The improved cycling stability of the tin phase can be explained by the reduced particle size because of the chemical interaction between $Li_4Ti_5O_{12}$ and the tin phase and the steric effect of $Li_4Ti_5O_{12}$ during the synthesis, as demonstrated in the previous section, and also the buffering effect of the porous $Li_4Ti_5O_{12}$ for accommodating the volume expansion of Sn during the charge/discharge processes.

Table 2
Cycling characterization of $Li_4Ti_5O_{12}$, SnO_2 and $Li_4Ti_5O_{12}$/tin phase composites calcined at 500 °C after 50 cycles (cutoff voltage: 0.5–3.0 V).

	Current density (mA g^{-1})	Initial/final capacity (mAh g^{-1})	Capacity retention (%)
$Li_4Ti_5O_{12}$/tin phase composite	100	303/226	74.6
	1000	214/203	94.8
	2500	176/106	60.2
Pure $Li_4Ti_5O_{12}$	100	211/196	92.9
	1000	173/167	96.5
	2500	139/131	94.2
Pure tin phase	100	403/50	12.4
	1000	50/8.7	17.4
	2500	7.8/6.5	83.3

4. Conclusions

$Li_4Ti_5O_{12}$/tin phase composites were successfully prepared by impregnation of the porous $Li_4Ti_5O_{12}$ matrix, which was synthesized by a cellulose-assisted combustion technique, with tin phase. Some chemical interaction between $Li_4Ti_5O_{12}$ and tin phase was likely created at a calcination temperature higher than 400 °C, which effectively suppressed the grain growth of tin phase during the calcination. On the other hand, the tin phase acted as a sintering aid of $Li_4Ti_5O_{12}$, such effect became noticeable at 700 °C. Therefore, a significant grain growth of $Li_4Ti_5O_{12}$ phase was observed at 700 °C. The formation of $Li_4Ti_5O_{12}$/tin phase composite increased the cycling stability of tin phase obviously but decreased the cycling stability of $Li_4Ti_5O_{12}$ slightly. The calcination at 500 °C resulted in the best electrochemical performance of the composites. The first discharge capacity was 442 mAh g^{-1} at current density of 100 mA g^{-1} between 0.5 and 3.0 V. The capacity was maintained 224 mAh g^{-1} after 50 cycles at 100 mA g^{-1} current density, due to the synergistic effect between $Li_4Ti_5O_{12}$ and tin oxide.

Acknowledgements

This work was supported by "Outstanding Young Scholar Grant" at Jiangsu Province under Contract No. 2008023 and the National Basic Research Program of China under Contract No. 2007CB209704.

References

[1] S. Megahed, W. Ebner, J. Power Sources 54 (1995) 155–162.
[2] M. Wakihara, Mater. Sci. Eng. R 33 (2001) 109–134.
[3] Y. Nishi, J. Power Sources 100 (2001) 101–106.
[4] B. Scrosati, Electrochim. Acta 45 (2000) 2461–2466.
[5] Y.P. Wu, E. Rahm, R. Holze, J. Power Sources 114 (2003) 228–236.
[6] G.B. Li, R.J. Xue, L.Q. Chen, Y.Z. Huang, J. Power Sources 54 (1995) 271–275.
[7] H. Abe, T. Murai, K. Zaghib, J. Power Sources 77 (1999) 110–115.
[8] K. Zaghib, M. Simoneau, M. Armand, M. Gauthier, J. Power Sources 81–82 (1999) 300–305.

[9] G.X. Wang, D.H. Bradhurst, S.X. Dou, J. Power Sources 83 (1999) 156–161.
[10] H. Ge, N. Li, D.Y. Li, C.S. Dai, D.L. Wang, Electrochem. Commun. 10 (2008) 719–722.
[11] L. Kavan, M. Gratzel, Electrochem. Electrochem. Solid State Lett. 5 (2002) A39–A42.
[12] P.P. Prosini, R. Mancini, L. Petrucci, V. Contini, P. Villano, Solid State Ionics 144 (2001) 185–192.
[13] K. Zaghib, M. Armand, M. Gauthier, J. Electrochem. Soc. 145 (1998) 3135–3140.
[14] C.M. Julien, M. Massot, K. Zaghib, J. Power Sources 136 (2004) 72–79.
[15] H.Y. Yu, X.F. Zhang, A.F. Jalbout, X.D. Yan, X.M. Pan, H.M. Xie, R.S. Wang, Electrochim. Acta 53 (2008) 4200–4204.
[16] C.M. Shen, X.G. Zhang, Y.K. Zhou, H.L. Li, Mater. Chem. Phys. 78 (2002) 437–441.
[17] T. Ohzuku, A. Ueda, N. Yamamoto, J. Electrochem. Soc. 142 (1995) 1431–1435.
[18] C.H. Chen, J.T. Vaughey, A.N. Jansen, D.W. Dees, A.J. Kahaian, T. Goacher, M.M. Thackery, J. Electrochem. Soc. 148 (2001) A102–A104.
[19] M. Venkateswarlu, C.H. Chen, J.S. Do, C.W. Lin, T.C. Chou, B.J. Hwang, J. Power Sources 146 (2005) 204–208.
[20] S.H. Huang, Z.Y. Wen, J.C. Zhang, X.L. Yang, Electrochim. Acta 52 (2007) 3704–3708.
[21] G.J. Wang, J. Gao, L.J. Fu, N.H. Zhao, Y.P. Wu, T. Takamura, J. Power Sources 174 (2007) 1109–1112.
[22] D. Aurbach, A. Nimberger, B. Markovsky, E. Levi, E. Sominski, A. Gedanken, Chem. Mater. (14) (2002) 4155–4163.
[23] L. Yuan, Z.P. Guo, K. Konstantinov, H.K. Liu, S.X. Dou, J. Power Sources 159 (2006) 345–348.
[24] H. Li, X.J. Huang, L.Q. Chen, J. Power Sources 81–82 (1999) 335–339.
[25] T. Brousse, S.M. Lee, L. Pasquereau, D. Defives, D.M. Schleich, Solid State Ionics 113–115 (1998) 51–56.
[26] Y. Kim, Y. Yoon, D. Shin, J. Anal. Appl. Pyrol. 85 (2009) 557–560.
[27] O. Crosnier, T. Brousse, X. Devaux, P. Fragnaud, D.M. Schleich, J. Power Sources 94 (2001) 169–174.
[28] G.X. Wang, J.H. Ahn, M.J. Lindsay, L. Sun, D.H. Bradhurst, S.X. Dou, H.K. Liu, J. Power Sources 97–98 (2001) 211–215.
[29] I. Sandua, T. Broussea, D.M. Schleicha, M. Danot, J. Solid State Chem. 177 (2004) 4332–4340.
[30] S.B. Yang, H.H. Song, H.X. Yi, W.X. Liu, H.J. Zhang, X.H. Chen, Electrochim. Acta 55 (2009) 521–527.
[31] M. Egashira, H. Takatsuji, S. Okada, J. Yamaki, J. Power Sources 107 (2002) 56–60.
[32] X.W. Zhang, C.S. Wang, A.J. Appleby, F.E. Little, J. Power Sources 109 (2002) 136–141.
[33] Y. Zheng, J. Yang, Y.N. Li, J.L. Wang, J. Power Sources 174 (2007) 624–627.
[34] E. Rönnebro, J.T. Yin, A. Kitano, M. Wada, T. Sakai, Solid State Ionics 176 (2005) 2749–2757.
[35] Y.J. Hao, Q.Y. Lai, Y.D. Chen, J.Z. Lu, X.Y. Ji, J. Alloys Compd. 462 (2008) 404–409.
[36] T. Yuan, R. Cai, K. Wang, R. Ran, S.M. Liu, Z.P. Shao, Ceram. Int. 35 (2009) 1757–1768.
[37] Z.R. Dai, Z.W. Pan, Z.L. Wang, Adv. Funct. Mater. 13 (2003) 9–24.
[38] B. Shen, X. Yao, L.P. Kang, D.S. Peng, Ceram. Int. 30 (2004) 1203–1206.
[39] M. Peiteado, J.F. Fernández, A.C. Caballero, J. Eur. Ceram. Soc. 25 (2005) 2999–3003.
[40] C.L. Huang, M.H. Weng, H.L. Chen, Mater. Chem. Phys. 71 (2001) 17–22.
[41] K. Nakahara, R. Nakajima, T. Matsushima, H. Majima, J. Power Sources 117 (2003) 131–136.
[42] J. Read, D. Foster, J. Wolfenstine, W. Behl, J. Power Sources 96 (2001) 277–281.